Journal of Power Sources 196 (2011) 10686–10691

Contents lists available at SciVerse ScienceDirect

Journal of Power Sources

journal homepage: www.elsevier.com/locate/jpowsour

Sn nanocrystal/carbon composites as high-capacity anode materials for lithium rechargeable batteries

Youngmin Lee, Yong-Mook Kang*

Division of Advanced Materials Engineering, Kongju National University, 275 Budae-dong, Cheonan, Chungnam, Republic of Korea

ARTICLE INFO

Article history:
Received 4 August 2011
Received in revised form 25 August 2011
Accepted 26 August 2011
Available online 2 September 2011

Keywords:
Sn nanocrystals
Chemical reduction method
Pinning effect
Carbon composite
Lithium rechargeable battery

ABSTRACT

High-capacity lithium-storage materials in metal composite form are being extensively researched, which can replace the carbon-based lithium intercalation materials currently commercialized as the negative electrode of lithium rechargeable batteries. Herein, Sn nanocrystals and Sn nanocrystal/carbon composites with various particle sizes are prepared by the chemical reduction method where surfactant can control the resultant particle size because the particle size of metal-based materials is the main underlying factor for their electrochemical enhancement. The chemical reduction approach using surfactants is very effective for varying the particle size of Sn nanocrystals. Sn nanocrystals with the optimized particle size in terms of anodic properties are made into a composite with carbon acting as an agglomeration preventer as well as an electronic conductor. The controlled size of the Sn nanocrystal in the carbon is associated with their drastically improved electrochemical performance retaining above 65% of the initial capacity after 30 cycles.

1. Introduction

Considerable effort has been devoted to the use of Sn based materials as alternative anodes to carbonaceous materials in lithium rechargeable batteries [1–6]. Even if commercialized carbon exhibits good compatibility with organic electrolytes desirable for a potential profile for Li-ion intercalation and good cycle life, its wider application has been limited by a low practical specific capacity below 372 mAh g^{-1}. Hence, high capacity alternatives such as Sn or Si based materials have thus become sought for. Even though Sn (theoretical capacity: 990 mAh g^{-1}) has been considered as one of the most attractive options for high energy density purposes, its poor cyclic properties have been delaying its commercialization. The poor cyclic behavior of Sn is associated with its alloying/de-alloying reactions, which involve large volumes changing during Li^+ insertion or extraction [7].

To exclude the cyclic degradation of Sn based materials related to volume expansion, various studies have been undertaken where the volume expansion and particle aggregation that worsen pulverization can be alleviated by adopting size control [8–10] or incorporating inactive matrices [11–16]. Amongst the various solutions, nanostructure control for Sn has been regarded as one of the most efficient methods of accommodating the unwanted volume change and thus preventing its electrochemical activity from being lost. Recently, many inorganic nanocrystals have been prepared by surfactant-assisted processes that permit outstanding control over the growth of metal oxide or metal nanocrystals, leading to almost perfectly mono-dispersed samples [17,18]. Additionally, the ability of the surfactants to cap the surface of the nanocrystals provides several advantages such as a low agglomeration tendency and good dispersion in organic solvents. Hence, in this study, the surfactant-assisted process has been adopted for efficient size control of Sn nanocrystals against their critical volume change during Li^+ insertion/extraction and carbon has been used as an adsorbing material to not only prevent agglomeration or size growth in the Sn nanocrystals but also supply kinetically unlimited electron transport.

2. Experimental

A Sn precursor solution was prepared by dissolving 0.2 g of $SnCl_2{\cdot}2H_2O$ (Aldrich) with 0.01 g poly(vinylpyrrolidone) (PVP, Mw = 55,000, Aldrich) or 0.1 g α-D-glucose (Aldrich) as a surfactant (surface active agent) in distilled water (25 ml). The solution was rapidly resolved by 0.067 g of $NaBH_4$ as the reducing agent for $SnCl_2{\cdot}2H_2O$ with vigorous stirring for 10 min. To remove the impurities, the final product was washed with ethyl alcohol through a centrifugal process and dried at 60 °C for 6 h in a vacuum oven. To synthesize the Sn nanocrystal/carbon composites, an Sn solution was prepared by dispersing synthesized Sn in ethyl alcohol (15 ml). Meanwhile, the carbon solution was prepared by dispersing 0.2 g carbon powder (~100 μm, Kanto Chemical) in ethyl alcohol (15 ml)

* Corresponding author. Tel.: +82 41 521 9378; fax: +82 41 568 5778.
E-mail addresses: dake1234@kongju.ac.kr, dake@kaist.ac.kr (Y.-M. Kang).

0378-7753/$ – see front matter © 2011 Elsevier B.V. All rights reserved.
doi:10.1016/j.jpowsour.2011.08.106

with vigorous stirring for 30 min. The Sn solution was added dropwise to the carbon solution under continuous vigorous stirring for 24 h. Then, the product was washed with ethyl alcohol through a centrifugal process and dried at 60 °C for 6 h in a vacuum oven.

To make electrodes for the electrochemical measurement, a mixture of 75 wt.% of each active material and 17 wt.% acetylene black was added to a solution containing 8 wt.% polyvinylidene fluoride (PVDF) in n-methyl-2pyrolidinone (NMP). This slurry was pasted onto a copper foil current collector and dried at 120 °C for 5 h in a vacuum (10^{-3} Torr). After pressing under a pressure of approximately 5000 psi, half cells (CR 2016 coin-type) were fabricated to evaluate the anodic performance of the resulting Sn based composites. A cell assembly was performed in an Ar-filled glove box with less than 10 ppm each of oxygen and moisture. A Li metal foil was used as the counter and reference electrodes, and 1 M of $LiPF_6$ dissolved in a 1:1 (v/v) mixture of ethylene carbonate (EC) and diethylene carbonate (DEC) was employed as the electrolyte. The charge–discharge tests on the Sn based nanocrystals or composites were performed for up to thirty cycles in the range of 0.05–1.5 V (vs. Li/Li^+). Sn based nanocrystals or composites were charged or discharged at 0.1 C in the constant current mode.

The microstructure and morphology of the Sn based materials were characterized by X-ray diffraction (XRD; Rigaku D/Max-RB diffractometer, using Cu Kα radiation at 40 kV and 100 mA), field emission scanning electron microscopy (FE-SEM; TESCAN MIRA

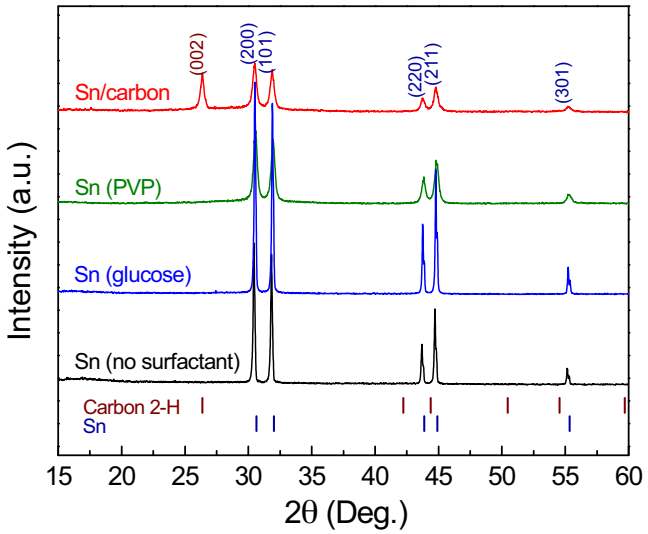

Fig. 1. XRD patterns of the Sn-based materials: Sn nanocrystals without surfactant (black line), Sn nanocrystals with α-D-glucose (blue line), Sn nanocrystals with PVP (green line), and Sn nanocrystal/carbon composites (red line). (For interpretation of the references to color in this figure legend, the reader is referred to the web version of the article.)

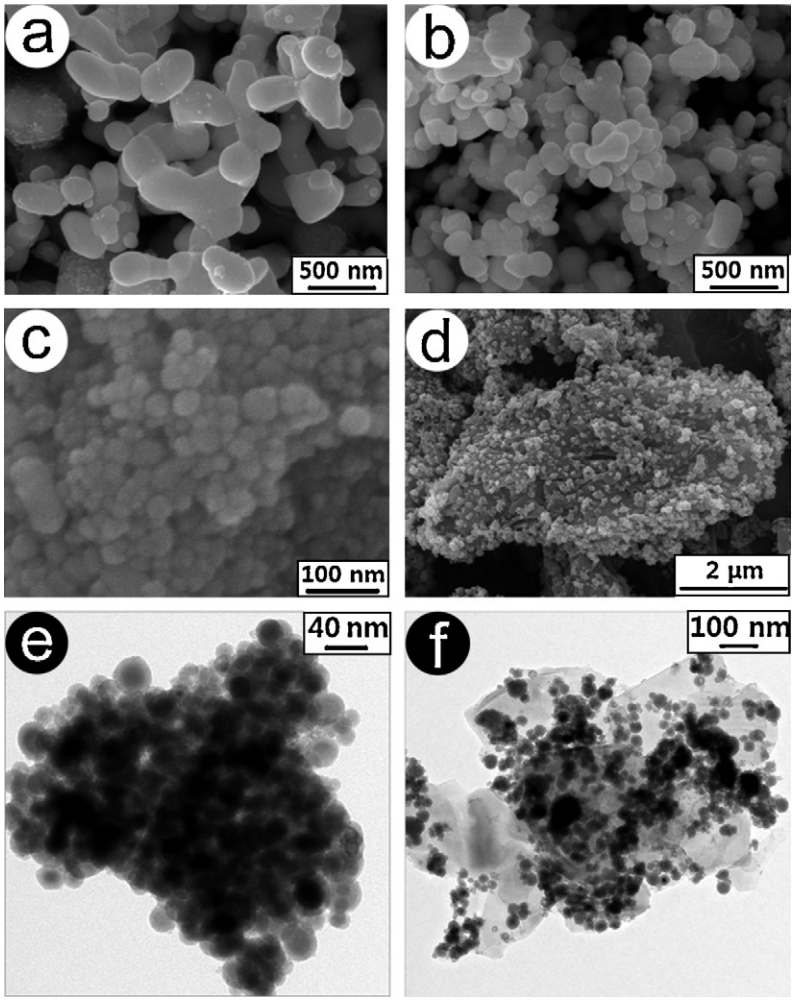

Fig. 2. SEM observations of (a) Sn without surfactant, (b) Sn with α-D-glucose, (c) Sn with PVP, and (d) Sn(PVP)/carbon composite. TEM observations of (e) Sn with PVP and (f) Sn (PVP)/carbon composite.

LMH2, operated at 15 kV), and high-resolution transmission electron microscopy (HR-TEM; Philips F20Tecai operated at 200 kV).

3. Results and discussion

Fig. 1 presents the XRD patterns of the Sn based materials synthesized without surfactant (black line in Fig. 1) or resulting from diverse surfactants such as glucose (blue line in Fig. 1) and PVP (green line in Fig. 1). The peak center and the full width at half-maximum (FWHM) of peak were determined by fitting the peak to the Lorentzian function. Each particle size was calculated using Scherrer's equation [19]. The resultant value of the crystallite size, obtained from the (2 0 0) strongest reflection, corresponds to more than 200 nm in pristine Sn nanocrystals, approximately 100 nm in those with glucose, and approximately 30 nm in those with PVP. As expected, the particle size of the Sn nanocrystals was successfully controlled in several tenths or hundredths of nanometer using the surfactant-mediated method. Because the electrochemical properties of Sn are determined by its particle size, the 30 nm Sn particles were chosen as the active sections of the Sn nanocrystal/carbon composites prepared by a direct reduction of $SnCl_2{\cdot}2H_2O$ onto carbon. The red line in Fig. 1 proves the existence of (0 0 2) peak attributed to the carbon in addition to the main peaks formed by the Sn nanocrystals.

Fig. 2(a)–(c) shows the SEM images of Sn based materials synthesized without surfactant (Fig. 2(a)) or surface-controlled using glucose (Fig. 2(b)) and PVP (Fig. 2(c)). As calculated using Scherrer's equation, the particle size of Sn was varied from 200 to 30 nm using surfactants such as glucose or PVP. The Sn particles from the surfactant-free process agglomerate, which leads to an arbitrary size distribution, whereas the surface-controlled Sn particles using a surfactant have a mono-dispersed distribution and maintain its spherical shape well [10,20–22]. Thus, it has been proven here that the surfactant can control the particle size of Sn. Fig. 2(d) presents the SEM images of the Sn nanocrystal/carbon composites where the Sn nanocrystals are uniformly absorbed onto the carbon surface. The TEM images of the Sn nanocrystals (surface-controlled by PVP) and Sn nanocrystal/carbon composites in Fig. 2(e) and (f) provide a clearer view with respect to the particle size and morphology of the Sn nanocrystals as well as the distribution of the Sn on the carbon surface of the Sn nanocrystal/carbon composites.

Fig. 3 compares Sn nanocrystals with Sn nanocrystal/carbon composites in terms of electrochemical performance. The initial galvanostatic profiles of the Sn nanocrystals and Sn nanocrystal/carbon composites are demonstrated in Fig. 3(a), in which the voltage is varied from 0.05 to 1.5 V vs. Li/Li^+. The galvanostatic profiles of the Sn nanocrystals without surfactant and surface-treated by glucose show similar voltage plateaus during the Li^+ insertion/extraction which are indicative of traces of phase transitions between the Li–Sn intermetallic compounds. The analogy between the surfactant-free Sn and glucose-treated Sn in the initial charge/discharge profile may be attributed to their similar particle size around 100–200 nm. The Sn nanocrystals surface-treated by PVP display sloping voltage profiles are different from the multi-step plateaus of the above-mentioned nanocrystals [24,25]. Herein, the disparity between the PVP-treated Sn and other Sn nanocrystals can be satisfactorily explained by the difference in the particle size because the smaller the particle size of electrode materials, the larger their surface area which induces more irreversible surface reactions attributable to electrolyte decomposition on surface. Fig. 3(b) shows the cyclic performances of the Sn nanocrystals and Sn nanocrystal/carbon composites. Even though the first discharge capacities of the Sn nanocrystals made without surfactant and with glucose come to 577 and 555 mAh g^{-1}, respectively, further cycling led to a drastic capacity decay to 49 and 39 mAh g^{-1} after 30 cycles. A similar cyclic behavior of the nanocrystals made without any surfactant and with glucose exemplifies that the particle size and morphology are the main physical factors to conclusively determine the anodic properties of nanocrystals. On the other hand,

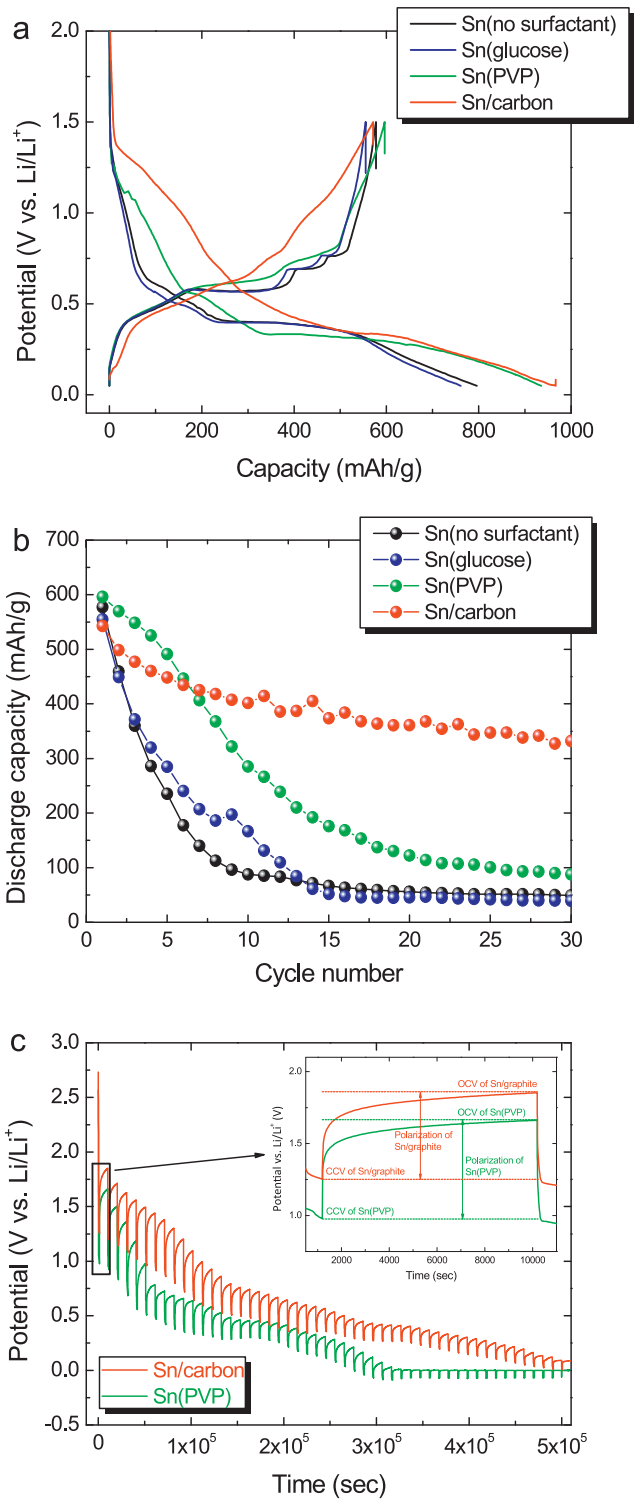

Fig. 3. (a) The initial galvanostatic charge/discharge profiles and (b) cyclic performances of Sn nanocrystals without surfactant or with various surfactants, and Sn nanocrystal/carbon composites. (c) Galvanostatic intermittent titration technique (GITT) curves for Sn nanocrystals and Sn nanocrystal/carbon composites during the first lithiation (the inset figure corresponds to the magnified rectangle part showing the polarization in details).

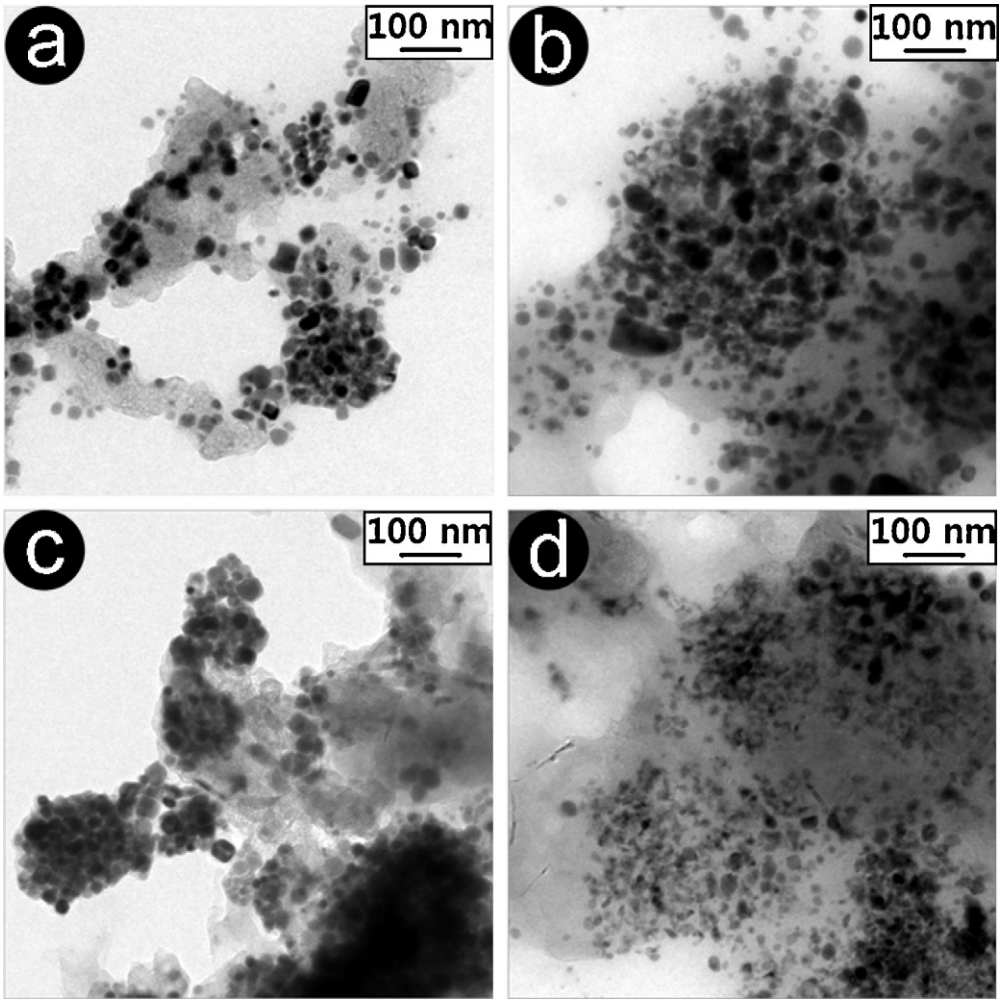

Fig. 4. TEM images of Sn nanocrystals and Sn nanocrystal/carbon composite after charge/discharge; the morphology of (a) Sn nanocrystals after 1st cycle (charge/discharge), (b) Sn nanocrystals after 10th cycle, (c) Sn nanocrystal/carbon composite after 1st cycle, (d) Sn nanocrystal/carbon composite after 10th cycle.

the Sn nanoparticle with PVP shows generally improved cyclic behavior compared with the other nanocrystals although its retained capacity is only 64 mAh g^{-1} after 30 cycles.

The essential problem encountered with nanocrystals is that their extremely small size is followed by a very high surface free energy leading to serious aggregation during electrochemical alloying or de-alloying with Li^+ and faces crucial pulverization. This means that controlling the particle size of Sn cannot be a fundamental solution for its anodic enhancement, and its aggregation during electrochemical reactions should be reduced. The proposed strategy for this is to adsorb the Sn nanocrystals onto the carbon acting as both an aggregation preventer and an electronic conductor. As shown in Fig. 3(a), the carbon causes the initial galvanostatic profile of the Sn nanocrystal/carbon composites to have a stronger slope, especially at high voltages around 1 V vs. Li/Li^+, indicating the increased unwanted electrolyte decomposition. Fig. 3(a) also demonstrates that the carbon marginally contributes to the charge or discharge capacity by intercalation or de-intercalation between its graphene layers. The initial discharge capacity is slightly lower compared with Sn nanocrystals, but it shows a greatly enhanced cyclic performance (65% after 30 cycles) implying that carbon can absorb material to prevent the agglomeration and pulverization of the Sn nanocrystals during the electrochemical reaction. To understand the electrochemical superiority of the Sn nanocrystal/carbon composites, the galvanostatic intermittent titration technique (GITT) curves were obtained during the initial Li^+ insertion into the Sn nanocrystals surface-treated by PVP and Sn nanocrystal/carbon composites (as seen in Fig. 3(c)). Here, the change of electrode resistances can be estimated from the disparity (polarization) between the open circuit voltages (OCV) and closed circuit voltage (CCV) at different states of charge (SOC) because the resistance is directly calculated by the polarization and applied current depending on Ohm's law: "$R = \Delta V$ (polarization)/I" [23]. At the beginning of the Li^+ insertion, a high polarization region exists, which is primarily related to solid-electrolyte interface (SEI) film formation from the electrolyte decomposition. The enlarged region of the Sn nanocrystal/carbon composites compared with the Sn nanocrystals may be associated with the increased electrolyte decomposition due to carbon. After this region, the polarization should decrease as the alloying of Sn with Li proceeds because Li–Sn intermetallic compounds feature high electronic conductivity. Furthermore, the alloying between Li and Sn involves the augmentation of the surface area, which is in inverse proportion to the resistance as indicated by "R (resistance) = ρ (resistivity) × L (length)/A (surface area)" [26]. However, the resistance of the Sn nanocrystals keeps increasing, which differs from the Sn nanocrystal/carbon composites conclusively indicating that the Sn nanocrystals themselves cannot abstain from the additional electrochemical degradation induced by pulverization due to the nanoparticle aggregation.

Fig. 4 indicates the detailed morphological changes of Sn nanocrystals ((a) and (b)) and Sn nanocrystal/carbon composites

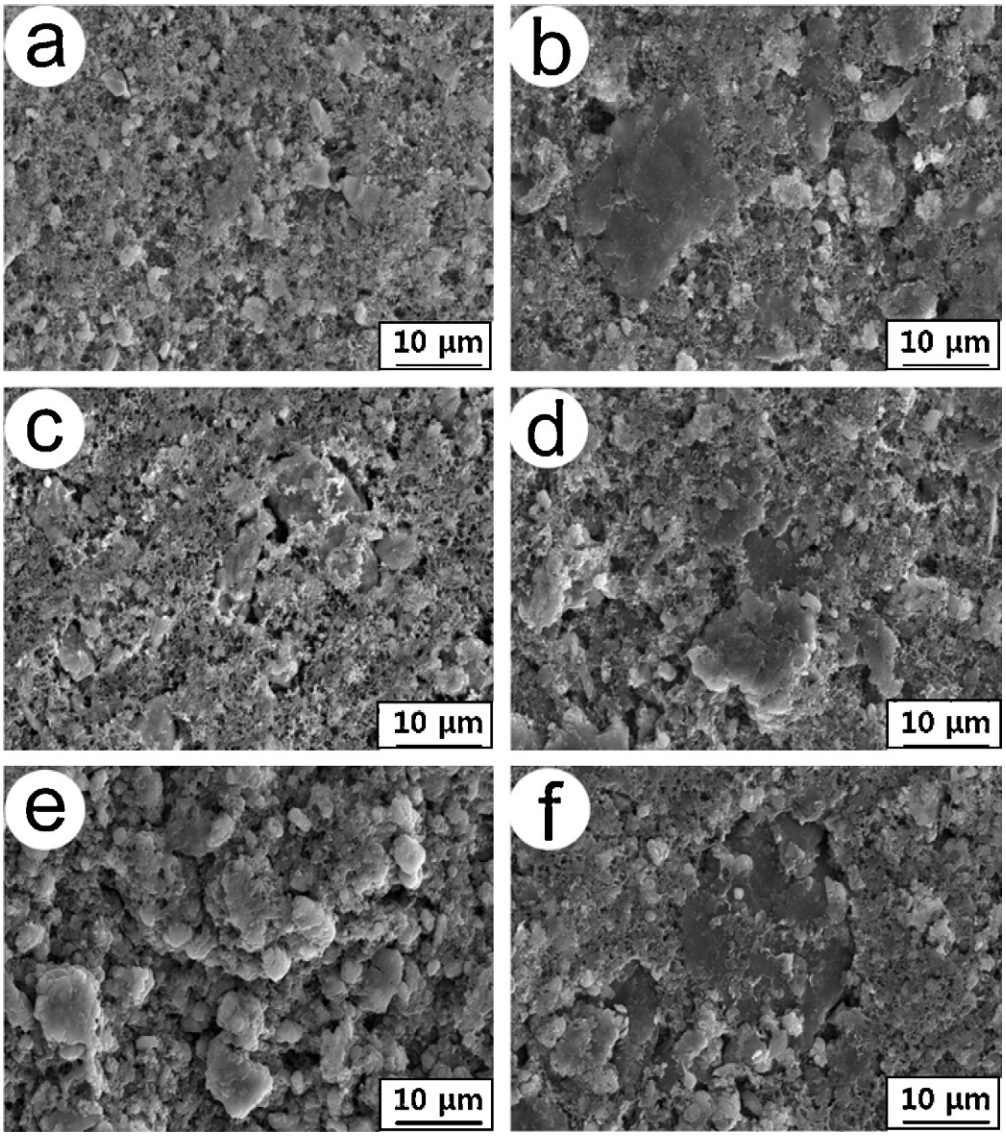

Fig. 5. Morphological difference between the electrodes each including Sn nanocrystals: (a) after 1st charge (Li^+ insertion), (c) after 1st cycle, (e) after 10th cycle and Sn nanocrystal/carbon composites: (b) after 1st charge, (d) after 1st cycle, (f) after 10th cycle.

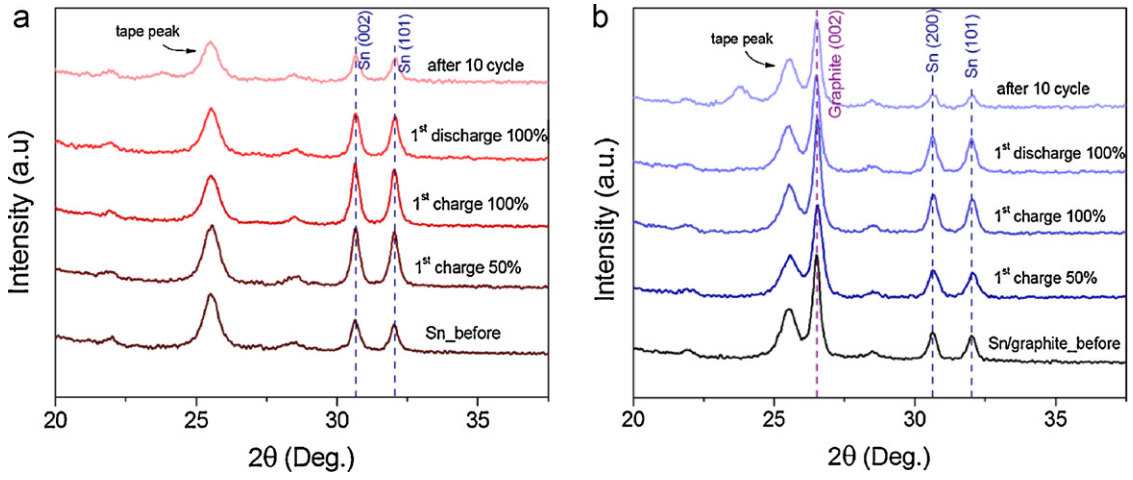

Fig. 6. XRD patterns of Sn nanocrystals electrode and Sn nanocrystal/carbon composites electrode as prepared state, after 1st charge (50% Li^+ insertion and 100% Li^+ insertion), after 1st cycle and after 10th cycle.

((c) and (d)). After 1st charge/discharge, Sn nanocrystals begin to aggregate into the larger particles with arbitrary shape and size (Fig. 4(a)), whereas Sn nanocrystals on carbon tend to maintain its initial shape and size (Fig. 4(c)). Because the charge/discharge is a typical exothermic reaction involving significant heat, the repetition of charge/discharge gives Sn nanocrystals enough activation energy to intensify their aggregation tendency as expected by GITT curves (Fig. 4(b)). Furthermore, the difference between Sn nanocrystals in size and shape gets larger under the influence of their pulverization after 10th cycle. In Fig. 4(d), Sn nanocrystals still show relatively uniform size distribution even if their general size gets smaller also due to the pulverization effect. Little aggregation of Sn nanocrystals in Sn nanocrystal/carbon composites proves that carbon plays the role of pinning medium preventing Sn nanocrystals from sticking to each other.

Fig. 5 demonstrates the effect of nanoparticle distribution on the morphological change of electrode during charge/discharge. After 1st Li^+ insertion (charge), the electrode containing Sn nanocrystals or Sn nanocrystal/carbon composites commonly show closely packed morphology induced by the initial volume expansion associated with Li–Sn alloying [27]. However, the morphological comparison between charged electrode and discharged electrode at 1st cycle indicates that Sn nanocrystal/carbon composites undergo less change than Sn nanocrystals probably due to significant pore concentration provided by carbon. The repetition of 10 times charge/discharge renders the size and shape of Sn nanocrystals arbitrary and makes considerable cracks on the electrode including Sn nanocrystals consequently depleting their electrochemical reactivity toward Li^+ (Fig. 5(e)). Meanwhile, Fig. 5(f) shows that morphological changes on the electrode of Sn nanocrystal/carbon composites are too small to evolve any electrochemical degradation in accordance with GITT curves and TEM observation.

Finally, XRD analyses were conducted to figure out the phase change correlated with morphological changes observed in SEM and TEM. Because the cycled electrodes were sealed with Sellotape to prevent air exposure, the peak related to Sellotape is observed around 26°. Fig. 6(a) shows that as 1st Li^+ insertion proceeds, the intensity of peaks indexed to Sn becomes significantly larger implying that Sn nanocrystals stick to each other with the help of exothermic heat. The drastically reduced peak intensity after 1st cycle and 10th cycle may result from the accelerated pulverization due to this aggregation tendency strengthened by low melting temperature of Sn. Sn nanocrystal/carbon composites do not have any distinct change not only in Sn peaks but also in carbon peak during charge/discharge except for a little diminution of Sn peaks after 10th cycle also attributed to pulverization. In accordance with SEM and TEM observations, carbon as a pinning medium helps Sn nanocrystals exempt from any detrimental aggregation worsening the electrochemical degradation in Sn nanocrystal/carbon composites. If carbon participates in charge/discharge process, the inter-planar spacing (d(002)) of its prismatic plane should be changed [28]. Because the (002) peak of carbon keeps up its initial position even during charge/discharge reaction, the primary role of carbon in Sn nanocrystal/carbon composites is not participating in the electrochemical reaction, but enabling Sn nanocrystals to retain their electrochemical reactivity. These consecutive analytic results based on TEM, SEM and XRD obtained from cycled electrodes or materials clearly stress out the significance of carbon as a pinning medium and a pore provider for the electrochemical superiority of Sn nanocrystal/carbon composites.

4. Conclusion

The particle size of Sn based materials has been proven to have significant physical characteristics for their anodic properties. Thus, to control the particle size of Sn, various surfactants are used during the chemical reduction of the Sn particles which result in the demonstration that PVP is the most appropriate material to enable the smallest particle size and most homogeneous size distribution. The selection of the PVP as the surfactant for Sn particles is also supported by the electrochemical superiority of the PVP-treated Sn nanocrystals as the anode material for lithium-ion secondary batteries. Finally, Sn nanocrystal/carbon composites obtained by the chemical reduction of Sn nanocrystals onto carbon display much more enhanced cyclic performance than the Sn nanocrystals as a result of the role of carbon as an aggregation preventer as well as an electronic conductor.

Acknowledgements

This work was supported by the Basic Science Research program (grant no. 20090072972), through the National Research Foundation of Korea funded by the Ministry of Education, Science, and Technology (NRF-2010-C1AAA001-0029018), and the Fundamental R&D Program for Technology of World Premier Materials funded by the Ministry of Knowledge Economy (grant no. 10037918).

References

[1] M. Winter, J.O. Besenhard, Electrochim. Acta 45 (1999) 31.
[2] Y. Idota, T. Kubota, A. Matsufuji, Y. Maekawa, T. Miyasaka, Science 276 (1997) 1395.
[3] N. Tamura, R. Ohshita, M. Fujimoto, M. Kamino, S. Fujitani, J. Electrochem. Soc. 150 (2003) A679.
[4] J.R. Dahn, A.K. Sleigh, H. Shi, J.N. Reimers, Q. Zhong, B.M. Way, Electrochim. Acta 38 (1993) 1179.
[5] R. Yazami, D. Guerard, J. Power Sources 43 (1993) 39.
[6] I.A. Courtney, W.R. McKinnon, J.R. Dahn, J. Electrochem. Soc. 146 (1999) 59.
[7] H. Huang, E.M. Kelder, L. Chen, J. Schoonman, J. Power Sources 81 (1999) 362.
[8] G.L. Cui, Y.S. Hu, L.J. Zhi, D.Q. Wu, I. Lieberwirth, J. Maier, K. Müllen, Small 3 (2007) 2066.
[9] H.S. Kim, J.P. Cho, J. Mater. Chem. 18 (2008) 771.
[10] Y. Wang, J.Y. Lee, Electrochem. Commun. 5 (2003) 292.
[11] C.C. Chang, S.J. Liu, J.J. Wu, C.H. Yang, J. Phys. Chem. C 111 (2007) 16423.
[12] J. Liu, W. Li, A. Manthiram, Chem. Commun. 46 (2010) 1437.
[13] A. Trifonova, M. Winter, J.O. Besenhard, J. Power sources 174 (2007) 800.
[14] J.Y. Lee, R. Zhang, J. Liu, J. Power sources 90 (2000) 70.
[15] L. Balan, J. Ghanbaja, P. Willmann, D. Billaud, Carbon 43 (2005) 2311.
[16] B.A. Boukamp, G.C. Lesh, R.A. Huggins, J. Electrochem. Soc. 128 (1981) 725.
[17] M.J. Noh, Y.J. Kwon, H.J. Lee, J.P. Cho, J.Y. Kim, M.G. Kim, Chem. Mater. 17 (2005) 1926.
[18] K.T. Lee, Y.S. Lee, S.M. Oh, J. Am. Chem. Soc. 125 (2003) 5652.
[19] A.L. Patterson, Phys. Rev. 56 (1939) 978.
[20] X.G. Peng, L. Manna, W.D. Yang, J. Wickhan, E. Scher, A. Kadavanich, A.P. Alivisatos, Nature 404 (2000) 59.
[21] J.W. Park, S. Rajendran, H.S. Kwon, J. Power sources 159 (2006) 1409.
[22] M.S. Park, Y.M. Kang, G.X. Wang, S.X. Dou, H.K. Liu, Adv. Funct. Mater. 18 (2008) 455.
[23] Y.M. Kang, S.M. Lee, S.J. Kim, G.J. Jeong, M.S. Sung, W.U. Choi, S.S. Kim, Electrochem. Commun. 9 (2007) 959.
[24] K.B. Kang, K.S. Song, H.S. Heo, S.Y. Yoo, G.S. Kim, G.H. Lee, Y.M. Kang, M.H. Jo, Chem. Sci. 2 (2011) 1090.
[25] K.T. Lee, J.P. Cho, Nano Today 6 (2011) 28.
[26] J.R. Macdonald, Impedance Spectroscopy: Emphasizing Solid Materials and Systems, John Wiley & Sons, New York, 1987.
[27] Y.M. Kang, M.S. Park, M.S. Song, J.Y. Lee, J. Power sources 162 (2006) 1336.
[28] Y.M. Kang, M.S. Park, J.Y. Lee, H.K. Liu, Carbon 45 (2007) 1928.